HAIT Journal of Science and Engineering, Volume 1, Issue 4, pp. 601-625

Crossover of a quantum dot with spin-orbit interaction in a high magnetic field to a quantum Hall ferromagnet *

Procolo Lucignano[1,2,*], Benoit Jouault[3] and Arturo Tagliacozzo[1,2]

[1] *Coherentia - Istituto Nazionale di Fisica della Materia (INFM), Monte S. Angelo - via Cintia, I-80126 Napoli, Italy*
[2] *Dipartimento di Scienze Fisiche, Università di Napoli "Federico II", Napoli, Italy*
[3] *Groupe d'Etude des Semiconducteurs, UMR 5650, Université Montpellier II, 34095 Montpellier, Cedex 5, France*
[*] *Corresponding author: procolo@na.infn.it*
Received 7 December 2004, accepted 12 March 2005

Abstract

Coulomb interactions of few electrons confined in a disk-shaped quantum dot, with a large magnetic field perpendicular to the dot, produce a fully spin polarized ground state. In the presence of an electric field also perpendicular to the dot and coupling spin and orbit (Rashba term), we find that the first excited state is a spin exciton with a reversed spin at the center of the dot. We explore the analogy with the quantum Hall ferromagnet at filling close to one, which is spin polarized and has skyrmions as collective low lying excitations. The energy of the spin exciton can be tuned with the electric field, and infrared radiation can provide energy and angular momentum to excite it. In the quantum dot the gap is finite and is tuned by the Rashba coupling. This opens up many unexpected possibilities of controlling the electron spin density at the dot and influencing the underlying nuclear spins via hyperfine interaction.

PACS: 73.21.La; 73.23.-b; 78.67.Hc

[*]Presented at Research Workshop of the Israel Science Foundation *Correlated Electrons at High Magnetic Fields*, Ein-Gedi/Holon, Israel, 19-23 December 2004

1 Introduction

Quantum dots (QD) [1] are good candidates for quantum computation in the solid state, provided quantum coherence can be preserved for sufficiently long times [2]. In a quantum dot, the confinement of electrons in restricted quasi-two-dimensional areas of a semiconductor heterostructure implies quantization of single particle levels. However, both the properties of an isolated QD and its sensitivity to the external fields and external contacts are ruled by the electron-electron interaction U. About a decade ago, control of a single electron charge was achieved by tuning a QD at Coulomb blockade [1]. Preserving the coherent superposition of single charges in solid state devices is, however, a formidable task, due to stray capacitances and uncontrolled charged defects.

On the other hand, much efforts is now being concentrated on manipulating the electron spin in a QD. Spin properties are quite relevant to conductance, in view of the possibility of spin blockade [3, 4], Kondo effect [5–7], or Berry phase induced tuning [8].

The coupling of the spin degree of freedom to the environment is weaker, and decoherence can occur on longer time scales. The relaxation rate of the longitudinal electron spin component $1/T_1$ is small because of reduced coupling of the electron spins to the phonons and of little role of spin-orbit coupling in impurity scattering [9, 10].

The most relevant mechanism of decoherence is expected to be hyperfine coupling of the dot electron spin density with the nuclear spins of underlying magnetic isotopes. In GaAs/GaAlAs structures there is some abundance of Ga and As isotopes with nuclear spin $I = 3/2$ and Al isotope with $I = 5/2$ and optical pumping of QD's nuclear spins has been demonstrated [11].

In this paper we discuss the spin properties of an isolated vertical QD in the presence of a magnetic field B in the $z-$direction, orthogonal to the dot disk (cylindrical symmetry is assumed). We also include the spin-orbit coupling (SO) induced by an electric field along z.

The reduction of the energy scale by a factor of 10^{-3} with respect to atoms, enhances the sensitivity of the electrons in the dot to an external magnetic field. We consider magnetic fields of the order of few Tesla, which reduces the role of the confinement potential and makes the QD conceptually not far from a quantum Hall disk when both the number of electrons N and B are increased. The quantum Hall disk becomes a quantum Hall ferromagnet (QHF) at odd integer fillings [12]. The ferromagnetic transition in the QHF is driven by orbital effects which are dominant in the cylindrical geometry [13]. Indeed, $e - e$ correlations relate orbital properties to spin

effects.

We show that by increasing B the total spin of the dot S increases up to its maximum $S = N/2$. The ground state (GS) of the dot becomes fully spin polarized (FSP). While the charge density is rather insensitive to the SO coupling, α, the latter couples the spin polarization to the orbital motion. The total angular momentum M and total spin component S_z are no longer individually conserved. This fact affects spin properties of the GS and the first excited states in a surprising way. Indeed, by increasing α, the expectation value of the spin density of the GS, which was originally oriented in the $z-$direction, acquires a component in the dot plane, because the minority spin density is increased and pushed from the center of the dot outward. Moreover, the combined effect of U and α deforms substantially the spin density of the first excited state (FES). A sharp minority spin polarization is present close to the dot center and the spin density heals back away from the origin with a node at some point ("spin exciton"). This situation is reminiscent of the case of the quantum Hall ferromagnet close to filling factor equal to one. There is evidence of skyrmion excitations in GaAs $2d$ electron gas systems close to such fillings by magnetoabsorption spectroscopy [14].

The spin exciton can be excited by means of far infrared radiation (FIR) [15]. Decoherence of the spin exciton in the presence of an environment of nuclear spins should be studied. In turn, the FIR excited spin exciton could act back on locally placed nuclear spins, which are, otherwise, weakly coupled to radiation. Nuclear spin relaxation $1/T_1$ can be changed by orders of magnitude by the gate voltage. When SO coupling is rather strong, as is the case we consider, $1/T_1$ is maximal at Coulomb blockade because it is inversely proportional to the electron escape rate from the dot [16].

Nuclear spins could constitute the basis for a qubit themselves [17] and our study adds information to the proposal that optically activated electron spins could manipulate the underlying nuclear spins [18].

On the other hand, a similar mechanism has been proposed for exploiting the QHF close to integer filling factors and the skyrmion excitation to manipulate the coherence of the nuclear spins [19, 20].

The paper is organized as follows. In Section 2 we summarize our results on the magnetic field dependence of the many-body states of the isolated dot with few electrons. The Hartree-Fock approach to the QHF and to the skyrmion excitation is reviewed in Section 3. In Section 4 we discuss the new features due to the spin-orbit coupling. In Section 5 we analyze the spin texture arising in the first excited dot state which we dub "spin exciton"

and compare it with the skyrmion of the QHF. In Section 6 we show that FIR could excite the spin exciton in the dot. The crossover to the QHF is signalled by the sharpening of the absorption edge in FIR.

2 Vertical quantum dot with azimuthal symmetry

The electrons of our dot are confined to a two-dimensional ($2d$) disk by a $2d$ parabolic potential and interact via the Coulomb repulsion whose strength is parametrized by $U = e^2/\kappa l$. Here l is the magnetic length in the parabolic confinement, $l = \sqrt{\hbar/m\omega_0}$ ($\omega_0 = \sqrt{\omega_d^2 + \omega_c^2(B)/4}$), and κ is the static dielectric constant [24]. In dots having a diameter of $\sim$ 100 nm, the level spacing and the Coulomb energy are of the order of $\sim$ 1 meV and most charging properties can be included within the Hartree-Fock (H-F) approximation, just like in atoms. Correlation effects do not alter significantly the picture for the charge, but may strongly influence the spin properties of the confined electrons. One striking evidence of this is the fact that Hund's rule [21], which is typical for atoms, is often satisfied in dots [22]. The Hund's rule is seen at work in Fig. 1 for $N = 4$ at B close to zero. The GS has $S = 1$ and $M = 1$. However, this is a fragile situation which disappears when B is increased [21, 23]. In fact B causes splitting of the single particle energies for $\pm|m|$ by preferring an orbiting direction (we choose B pointing downward which selects positive m values). Further increase of B selects GSs with large M, S as seen in Fig. 1 till the maximum $S = N/2$ is reached (fully spin polarized (FSP) state). This leads to successive crossing of dot levels. Note that we are not including a Zeeman spin splitting term which favours alignment of the electron spin along the z direction. Beside being very small in relevant cases, this term only lifts the spin degeneracy and has no other influence on our arguments. The Slater determinant which dominates the FSP GS is depicted in Fig. 2b for $N = 5$.

In Figs. 1 and 2 the boxes represent single particle wavefunctions of the two-dimensional harmonic confining potential in the external B field along $\hat{z}$:

$$\Psi_{n,m}(\rho, \theta) = \frac{e^{im\theta}}{l\sqrt{\pi}}\, R_{n|m|}(t) \quad . \tag{1}$$

Here n, m are the orbital quantum numbers and $t = \rho^2/l^2$. The radial wavefunction in Eq. (1) is expressed in terms of the Laguerre polynomials

L_ν^μ as:

$$R_{n|m|}(t) = \left[\frac{\left(\frac{n-|m|}{2}\right)!}{\left(\frac{n+|m|}{2}\right)!} \right]^{\frac{1}{2}} \quad e^{-\frac{t}{2}}\, t^{|m|/2}\, L^{|m|}_{\frac{n-|m|}{2}}(t) \quad . \tag{2}$$

We label the single electron states in the dot as $|n, m, s = \frac{1}{2}, s^z\rangle$ (s, s^z are the electron spin and its z-component).

The increase of the total spin S was measured in a dot with about 30 electrons, a striking evidence of e-e correlations [25]. When this happens, the dot acquires also the maximum possible density, a way of reaching some kind of incompressibility.

We use exact diagonalization for few electrons in the basis of states given by Eq. (2) [3], to discuss the spectral properties of the FSP dot which is stabilized by the Coulomb interaction.

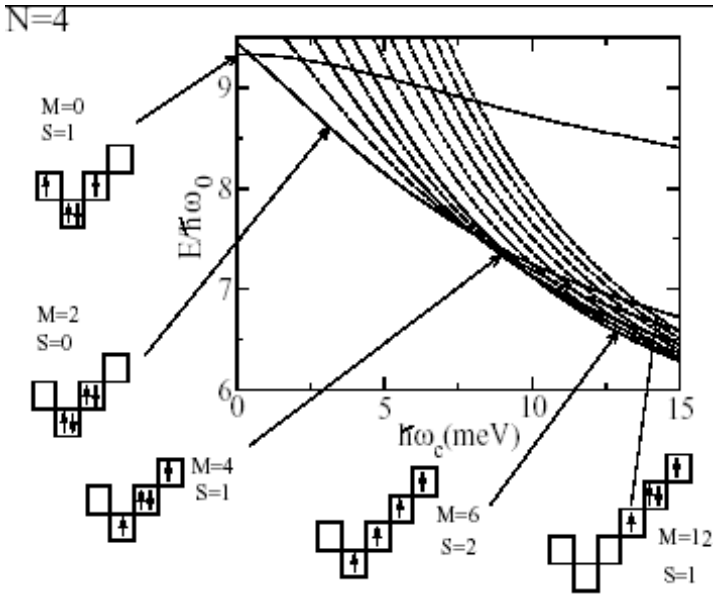

Figure 1: Crossing to higher M and higher S states with increasing magnetic field B for an isolated dot with $N = 4$ electrons. Hund's rule at $B = 0$ selects the $S = 1$, $M = 1$ state as the GS. Slater determinants giving the dominant contribution to the GS are depicted. Spins depicted here are reversed with respect to the rest of the paper because of the different conventions used in [21].

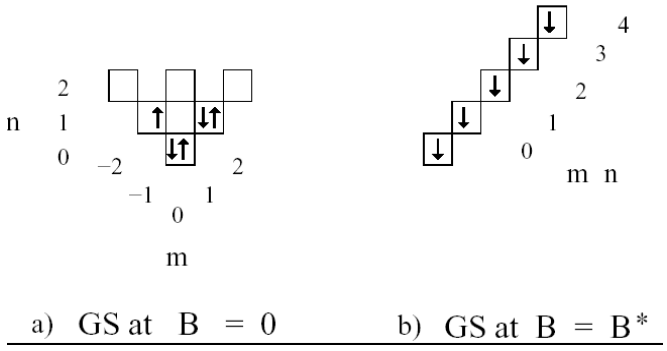

Figure 2: Slater determinants quoted in the text. Quantum numbers are $N = 5$, $S = 1/2$ for the state at $B = 0$ [a)] and $S = 5/2$ for the state at $B = B^*$, the magnetic field value at which the maximum absolute value of S is achieved [b)].

In Fig. 3 [left panels], we show the lowest lying total energy levels at fixed angular momentum M, versus M, for $U = 13$ meV and three values of B for a 5 electron dot. These are $B = 5$ meV [top], $B = B^* = 7$ meV [middle], $B = 11.5$ meV [bottom]. At each M, the spin degeneracy is marked by dashes of different length: short dashes for $S = 1/2$ (doubly degenerate level), medium dashes for $S = 3/2$ (fourfold degeneracy) and long dashes for $S = 5/2$ (sixfold degeneracy). On the r.h.s. of the picture the radial charge density of the corresponding GS is plotted versus the distance r from the dot center. Fig. 3 ([left panels]) shows that the levels cross with increasing B when M or S increases. At $B = B^* = 7$ meV the FSP GS is reached. Its Slater determinant is depicted in Fig. 2b and corresponds to $M = \sum_0^{N-1} m = 10$.

We concentrate on the GS state at $B = B^*$: this corresponds to the "maximum density droplet" state discussed in the literature [26]. Qualitatively we can say that at $B = B^*$ the dot attains its smallest radius.

As can be seen from the GS charge density, further increase of B leads to the so-called reconstruction of the charge density of the dot: an annular local maximum of the density is produced at the edge of the dot [27]. The breaking of azimuthal symmetry, which appears in the de Chamon-Wen phase [28], is not seen here because our single particle basis includes only azimutally simmetric wavefunctions. The M of the GS increases further, but S is no longer at its maximum. In the bottom panel of Fig. 3 it is shown that at $B = 11.5$ meV the GS energy is now achieved for $M = 13$

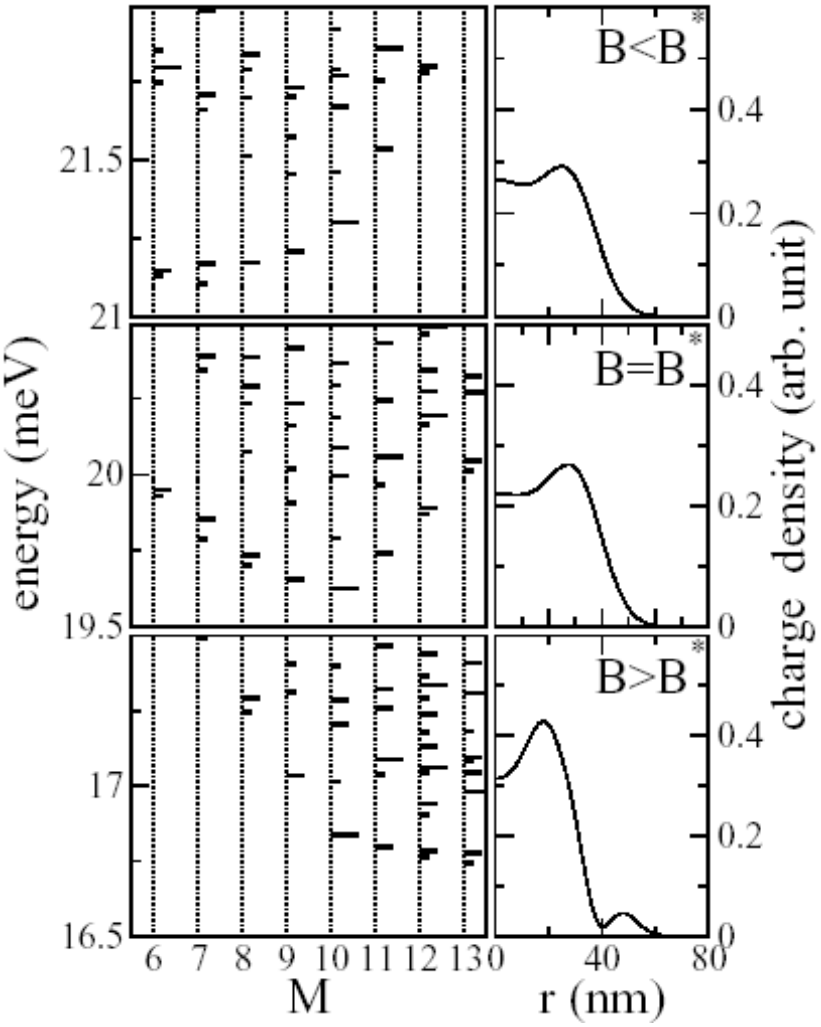

Figure 3: Energy levels without SO coupling for the dot with $N = 5$ electrons at $U = 13$ meV and $\omega_d = 5$ meV. Magnetic field values are: (in units of $\hbar\omega_c$) $B = 5$ meV [top], $B = B^* = 7$ meV [middle], $B = 11.5$ meV [bottom]. The total M is on the x axis. The levels are drawn with short, medium or long dashes, depending on the total spin: $S = 1/2, 3/2, 5/2$. In the right panels the corresponding charge density vs radial distance is plotted. From [24].

with a doublet ($S = 1/2$) state.

3 The quantum Hall ferromagnet

The GS of the QD at $B = B^*$ can be compared with a fully spin polarized quantum Hall state at integer filling. In the latter case, the GS is known to be ferromagnetic even in the limit of zero Zeeman spin splitting [29]. In the quantum Hall ferromagnet (QHF) the single particle Landau levels are:

$$\epsilon_{\nu,m} = (2\nu + |m| + 1)\hbar\omega_o - \frac{m}{2}\hbar\omega_c \tag{3}$$

where $\nu = (n - |m|)/2$ and $\omega_o = \sqrt{\omega_d^2 + \omega_c^2/4}$. If there is no confinement potential ($\omega_d = 0$), all ϵ_{0m} are degenerate. We neglect the Zeeman spin splitting. Indeed, the cyclotron frequency ω_c includes the effective mass and the Landau level separation is increased by a factor of ~ 20, while Zeeman spin splitting, being reduced by a factor of 4 in the semiconductor environment, becomes negligible in comparison [30]. The total angular momentum in a disk geometry is $M = N(N-1)/2$. In the Slater determinant for the LLL all angular momenta states with $\nu = 0$ and $m \geq 0$ are occupied once up to $m_{max} = N - 1$ (see Fig. 2b, where the single particle levels are taken as non-degenerate):

$$\left| QHF, 0 \right\rangle = \prod_{0 \leq m \leq N-1} \hat{a}^\dagger_{0m\downarrow} \left| vac \right\rangle . \tag{4}$$

Here $|vac\rangle$ is the vacuum state and $\hat{a}_{\nu=0m\sigma}$ are the single particle fermion operators associated to the LLL wavefunctions $f_{\nu=0m}\chi_\sigma$ (here χ_σ denotes the spin 1/2 wavefunction). They are derived from the orbitals Ψ_{nm} of Eq. (1), but with Laguerre polynomials $L_0^{|m|}(t) = 1$. This Slater determinant can be adopted as the GS of the QHF and gives a charge density which is flat as a function of the radius r, up to the disk edge $R_d \sim (2m_{max})^{1/2} l$. From R_d outward, it rapidly falls down to zero. In the dot case this feature is lost because of the presence of U, together with the fact that the number of electrons is small.

It was pointed out long ago [31] that, if the filling factor is slightly less than one, the first excited state can be a very special collective excitation with $S < N/2$ and an extra node in the spin density. The spin polarization is reversed at the center, but gradually heals to the dominant spin background over a distance of many magnetic lengths (SK state). For the hard

core model the HF equations can be solved analytically [32] and the Slater determinant $|S,K\rangle$ that describes this state conserves total J_z. We define the rotated fermion operators:

$$\begin{aligned} \hat{q}_j &= u_j\ \hat{a}_{0j-\frac{1}{2}\uparrow} + v_j\ \hat{a}_{0j+\frac{1}{2}\downarrow}\ , \qquad j \in (\frac{1}{2}, ...\infty)\ , \\ \hat{p}_{-\frac{1}{2}} &= \hat{a}_{00\downarrow}\ , \\ \hat{p}_j &= -v_j\ \hat{a}_{0j-\frac{1}{2}\uparrow} + u_j\ \hat{a}_{0j+\frac{1}{2}\downarrow}\ , \qquad j \in (\frac{1}{2}, ...\infty)\ . \end{aligned} \tag{5}$$

Normalization requires that $|u_j|^2 + |v_j|^2 = 1$. Note that the operator $\hat{p}_{-\frac{1}{2}}$ still belongs to the LLL as it destroys a particle in the $f_{\nu=0,m=0}\chi_\downarrow$ state. The generic Slater determinant built by means of these operators is:

$$|S,K\rangle = \prod_{j=\frac{1}{2}}^{\infty} \left(\hat{p}_{j-1}^\dagger\right)^{n_{j-1}^p} \left(\hat{q}_j^\dagger\right)^{n_j^q} |vac\rangle, \tag{6}$$

n_j^β are the occupation numbers of the single particle states. The state of Eq. (6) is labeled by the total spin S and by the number of flipped spins K. S_z is no longer a good quantum number and is substituted by

$$K = S + \frac{1}{2}\sum_{j=\frac{1}{2}}^{N-\frac{1}{2}} (n_j^q - n_{j-1}^p)\ . \tag{7}$$

The GS of Eq. (4) is obtained from Eq. (6) by taking $n_j^p =< p_j^\dagger p_j >= 1$ up to $j = N/2$ and all $n_j^q =< q_j^\dagger q_j >= 0$ together with $u_j = 1$. This is the state $|S = N/2, K = 0\rangle$ of Eq. (4) and is depicted in Fig. 4a. By analogy with Figs. 1 and 2, we use boxes to allocate electrons. Each box is cut into a lower and an upper triangle related to the diagonal, corresponding to the q and the p state of a given j_z, respectively. A heavy dot marks occupied orbitals.

In Fig. 4b we depict the first excited state $|S = N/2, K = 1\rangle$. The prefactors are given by

$$|u_j|^2 = 1 - |v_j|^2 = \frac{\xi^2}{\xi^2 + (j+\frac{1}{2})}\ , \tag{8}$$

where ξ is a length scale to be determined by minimizing the energy.

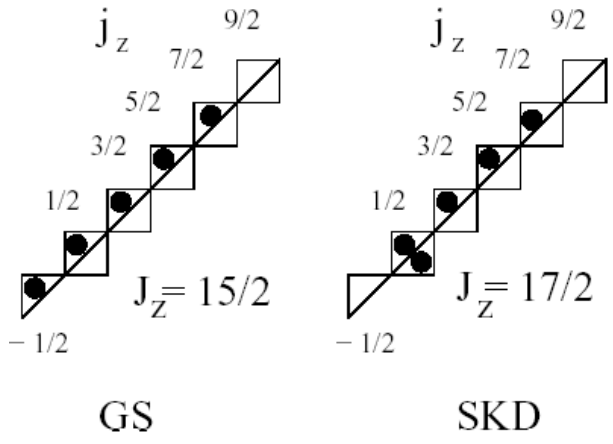

Figure 4: Slater determinants quoted in the text with the same labels. Quantum numbers are $N = 5$, $S = 5/2$ and J_z. Upper/lower triangles refer to single particle states labeled by j_z and p/q. Other possible quantum numbers do not appear. The dots mark occupied states. Configuration labeled as a) is involved in a state belonging to a much higher energy.

It can be shown [24] that, provided $j + \frac{1}{2} \sim r^2/l^2$, the choice of Eq. (8) leads to the skyrmion radial spin density:

$$s_x(\vec{r}) = \frac{2x\xi}{r^2+\xi^2}; \qquad s_y(\vec{r}) = \pm\frac{2y\xi}{r^2+\xi^2}; \qquad s_z(\vec{r}) = \frac{r^2-\xi^2}{r^2+\xi^2}\ . \tag{9}$$

The skyrmion is the topological excitation of the $O(3)$ $NL\sigma M$ in *2d* [33]. It is a finite action configuration, satisfying the classical equations of motion for the magnetization of the $NL\sigma M$, conserving $\vec{J} = \vec{S} + \vec{M}$ and belonging to a non trivial homotopy class. A disk of infinite radius in coordinate space can be compactified to a sphere S^2 in $\mathcal{R}^3$ having the origin in the south pole and the point at infinity in the north pole. A similar compactification can be performed in the order parameter configurational space. A uniform magnetization "down" is represented by a vector pointing to the south pole everywhere on S^2. If the topological charge is $Q = 1$, the shape of the magnetization field is $\vec{s}(\vec{r}) = \hat{r}$, where $\hat{r}$ is the normal to S^2 at each point. Q is the flux of $\vec{s}(\vec{r})$ through the sphere of unit radius. The spin polarization is "up" at the south pole and turns over continuously in space, until it reaches "down" at the north pole. That is, the spin polarization is flipped at the origin of the disk with respect to the GS and turns smoothly over away from it in the radial direction.

The $\pm$ in Eq. (9) refers to the sign of the topological charge $Q = \pm 1$:

$$Q = \frac{1}{8\pi} \int d^2x \; \epsilon_{\mu\nu} \vec{s} \cdot (\partial_\mu \vec{s} \times \partial_\nu \vec{s}) \quad . \tag{10}$$

We will show that a similar FES can be enforced in the QD by the SO coupling.

4 Adding the SO interaction to the QD

The confinement of the electrons in the $x - y$ plane implies the presence of an electric field in the $z-$direction, provided by the band bending of the heterostructure. This gives rise to the so called SO Rashba term [34], which can be enhanced even further by applying an extra gate on top of the vertical structure. The term to be added to the Hamiltonian is: [34]:

$$H_{so} = \frac{\alpha}{\hbar} \left[\left(\vec{p} + \frac{e}{c} \vec{A} \right) \times \vec{\sigma} \right] \cdot \hat{z} \; . \tag{11}$$

Here $\vec{\sigma}$ are the Pauli matrices, $\vec{A}$ is the vector potential due to the magnetic field: $\vec{A} = B/2 \; (-y, x, 0)$ and α (with dimensions of eVÅ) includes the effect of an electric field $\mathcal{E}$. The SO couples together states $|n', m+1, s = \frac{1}{2}, \downarrow\rangle$ with $|n, m, s = \frac{1}{2}, \uparrow\rangle$ as well as $|n', m-1, s = \frac{1}{2}, \uparrow\rangle$ with $|n, m, s = \frac{1}{2}, \downarrow\rangle$. While s_z and m are no longer separately conserved, their sum $j_z = s_z + m$ (with a half integer j_z) is a good quantum number.

The SO term lifts the degeneragy of the J multiplet by producing a linear splitting ~ 0.1 meV each 20 meVÅ. Linearity holds only for small α's. When U is relatively large, the multiplet is "normal", that is the state with $J_z = M - S_z$ is lowest in energy. This reminds what happens in atoms when a shell is less than half filled.

The SO couples all states corresponding to equal J_z belonging to different multiplets. In particular, for the case of $N = 5$ at $B \sim B^*$, which is reported in Fig. 3 (middle) these are all states at the left of the lowest lying one. Thus, the GS with $J_z = 5/2$ is an admixture of $(M = 7, S = -1/2)$,$(M = 6, S = -3/2)$,$(M = 5, S = -5/2)$. They are all within 1 meV, which is an energy interval that can be spanned by a SO coupling $\alpha > 200$ meVÅ. This value can be easily obtained in actual devices. Indeed, by applying external gate voltage orthogonal to the XY plane, in the case of dot made of III-V semiconductor heterostructures, it is now possible to tune continuosly α from few tenth of meVÅ to more than 300 meVÅ.

As the low lying levels are quite packed close to B^* (see, e.g., Fig. 1), a marked anticrossing between levels of equal J_z follows.

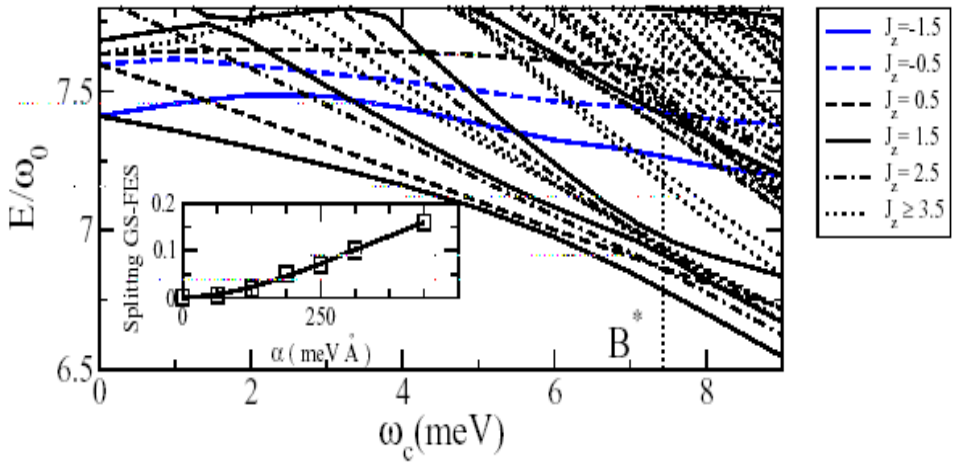

Figure 5: N=3 particles dot: energy spectrum vs magnetic field ω_c in the presence of SO. $\omega_d = 7$ meV, $U = 13$ meV, $\alpha = 250$ meVÅ. The GS is $J_z = 3/2$, the FES is $J_z = 5/2$. Inset: GS-FES spin gap vs α at $\omega_c = 8$ meV for N=3.

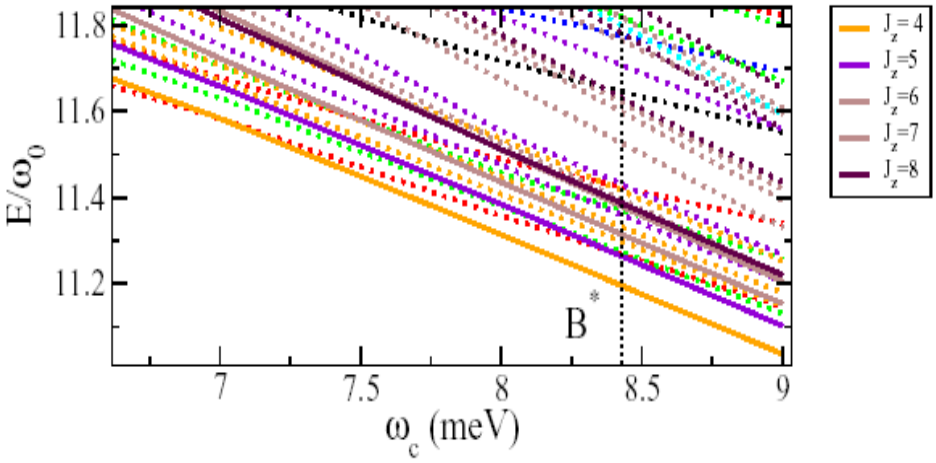

Figure 6: N=4 particles dot: energy spectrum vs magnetic field ω_c in the presence of SO. The GS is $J_z = 4$, the FES is $J_z = 5$. $\omega_d = 7$ meV, $U = 13$ meV, $\alpha = 250$ meVÅ.

In Figs.5,6 the anticrossings for $N = 3$ and $N = 4$ as seen from Figs. 5 and 6 are shown. However, by increasing the number of particles the level structure becomes richer and the typical appearance of anticrossings fades away. In fact, for $N = 4$, anticrossings are less prominent and the level separation of the bunch of states in Fig. 6 is much smaller. Nevertheless a gap develops at $\omega_c \approx 5.5$ meV between the GS ($S = 2, J_z = 4$) and the FES ($S = 1, J_z = 5$), originating from the $M = 6$ multiplet. The gap is strongly sensitive to the SO tuning and increases with increasing α (see inset in Fig. 5). The J_z of the FES is increased by one unit with respect to that of the GS.

While the charge density is rather insensitive to the increase of B or α close to the maximum density droplet condition (provided the dot charge does not reconstruct), the radial spin density $\vec{s}(r)$ strongly depends on B. In the absence of SO, the orientation of S was undetermined in the FSP GS, provided that neither the Zeeman spin splitting nor the SO is included. Zeeman spin splitting would orient the spin magnetization $\langle S_z(r)\rangle$ of the GS downward. When the SO is added, the $z-$component of the total spin is no longer well defined and some admixture of up and down spins appears. The Rashba coupling acts as an effective *in plane* magnetic field that forces a precession of electron spins in the dot plane. On the other hand, B is orthogonal to the plane and tends to tilt the spin out of the plane, contrasting the Rashba coupling. Our calculation confirms the intuitive idea that the SO coupling is weakened by an orthogonal magnetic field: this can be seen by monitoring the matrix elements of the interaction versus B.

Pictorially, one can imagine that the SO coupling tends to shift the $\downarrow$ spin density, related to the $\uparrow$ one, radially outward.

Classically, one can think of a particle constrained by incompressibility of the maximum density droplet condition to rotate at the disk boundary with the velocity $v = v_\vartheta = R\dot{\vartheta}$ in the magnetic field B. The particle experiences a radial Lorenz force $F_r = eBr\dot{\vartheta}/c$. The parabolic confinement potential acts as an effective small radial electric field ϵ_r at the dot boundary, which balances F_r at $r \approx R$. According to the SO term of Eq. (11), the energy of particles with spins up and down differ by

$$\Delta\epsilon_Z \propto \frac{e\epsilon_r R^2}{\hbar}\left(p_\vartheta + \frac{e}{c}A_\vartheta(r)\right)\sigma_z = \hbar\frac{R^2}{l^2}\,\dot{\vartheta}\left(m + \pi\frac{Br^2}{\phi_o}\right)\sigma_z\ , \qquad (12)$$

(where $\phi_o = hc/e$ is the flux quantum). This spin dependent term favours a radial displacement of particles of opposite spin at the boundary.

According to this argument, the role of U is quite substantial. Numerical results show that the J_z multiplet is not ordered as "normal" for

low U values. Besides affecting the energy of the states, the effect of U is to enhance the transfer of weight from the majority ("down") to the minority ("up") spin population. This is shown in Fig. 7 [24], where the occupation numbers $n_{n=m,m,\sigma} = \langle |c^{\dagger}_{nm\sigma} c_{nm\sigma}| \rangle$ are reported for the states $|J_z = 15/2, 17/2, 25/2 >$, for $U = 0$ [left panels] and $U = 13$ meV [right panels], respectively.

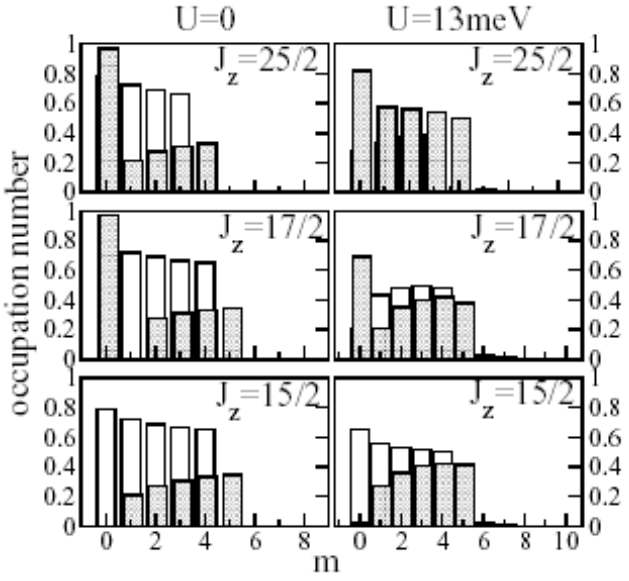

Figure 7: The occupation numbers $n_{n=m,m,\sigma}$ in the state at $J_z = 15/2, 17/2, 25/2$ for small U [$left$], and large U [$right$] ($\alpha = 250$ meVÅ). White bars refer to spin down, grey bars refer to spin up. We stress that at $U = 0$ the ordering level energy corresponding to the three panels on the left is changed compared to the ones on the right ($U = 13$ meV) and the level marked by $J_z = 15/2$ lies quite high in energy when $U = 0$.

In QH systems the interplay of the Zeeman interaction and the e-e interaction determines the size of skyrmion state. Here we have neglected the Zeeman term. However, according to Eq. 12, the SO term plays similar to that role of the Zeeman term in splitting the single particle spin levels, because of the presence of the confining potential. As the SO coupling is substantial, such a perturbation is overwhelming with respect to the Zeeman spin splitting and it constitutes the leading effect in determining the size of

FES skyrmion-like spin distribution.

The charge and spin polarization densities of the GS at $N = 5$ ($J_z = 15/2$), for $U = 13$ meV, are compared in Fig. 8 for three values of the SO coupling. As it appears from the top panel, the charge density of the GS is only mildly changed when we increase the SO coupling. $\langle S_z(r) \rangle$ tends to flatten in the GS.

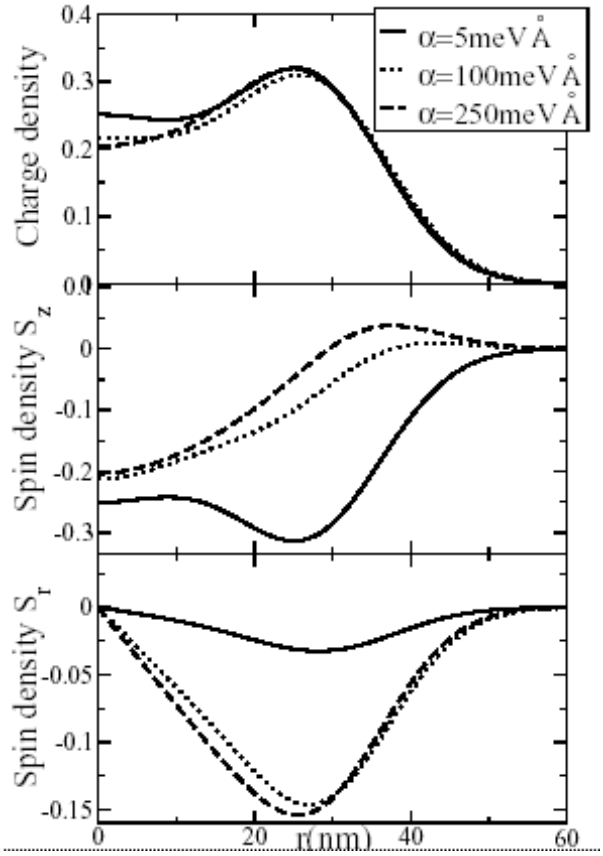

Figure 8: Charge density, azimuthal spin density S_z, in-plane spin density S_r in the radial direction for the GS ($N = 5$, $J = 15/2$) at various SO couplings: $\alpha = 5, 100, 250$ meV Å. Here $B = 7$ meV, $U = 13$ meV, and $\omega_d = 5$ meV.

5 Comparison between the spin exciton and the skyrmion

In this section we give arguments supporting our claim that the FES of the dot at B^* corresponds to the state $|N/2, 1\rangle$ in the QHF limit, that is in the limit of zero confinement potential and filling factor less than one. The comparison is in order, because the physics of the dot turns into that of a quantum Hall disk by increasing the magnetic field, as long as the ratio $\omega_d/\omega_c \to 0$. Of course, while the infinite quantum Hall system is marked by a phase transition to the spin polarized state, the dot, being a system with a finite number of particles, undergoes a crossover to the FSP state which is not a broken symmetry state.

In Fig. 9 we show the charge and spin densities of the complete GS multiplet for $N = 5$ at $\alpha = 100$ meVÅ, $U = 13$ meV and $B = B^*$. The situation is quite peculiar: by looking at $< S_z >$ [middle panel], we see that the GS has a down spin density everywhere in the dot, except for a little reversed tail at the boundary. By contrast, the highest energy state of the multiplet with $J_z = 25/2$ has an up spin density at any r. The FES state, being intermediate between the two, displays a reversed spin at the center of the dot but the spin polarization changes into down when approaching the edge, to restore the spin density of the GS. There is a node in the middle! By contrast, other states (19/2, 21/2, 23/2 and 25/2) are rather featureless. The trend is confirmed by looking at the projection of the spin density in the plane of the dot $S_r = \hat{r} \cdot \vec{S}$ (see Fig. 9 [bottom panel]). This is the information complementary to $S_z(r)$. When $S_r(r)$ is strongly non zero, then $S_z(r)$ is heavily reduced.

The radial distribution of the spin density in FES recalls the one of Eq. (9) except for a very shallow tail at the boundary. It is remarkable that close to the origin the radial component of the spin density $S_r(r)$ in FES keeps flat, contrary to other parameters. This marks full spin reversal at the origin with respect to the GS. Away from the center the spin polarization of the FES state lines up gradually with the one of the GS as it happens for the case of skyrmions.

Correspondingly, there is a piling up of the charge at the origin (see Fig. 9 [top panel]) associated to the locally dominant down spin density. However, it has a little weight in integrating over the volume.

The FES is a collective excitation of the QD which we call a "spin exciton". As in the case of the skyrmion, $S_z(r)$ has an extra node at $r = \xi$. In the dot case the length scale ξ is no longer arbitrary, but is fixed by the

strength of the SO coupling. The latter breaks artificially the symmetry for separate rotations in real space around the $z-$ axis and rotations in the spin space, but keeps $J_Z = M + S_z$ as a good quantum number, exactly as it occurs for the skyrmion in the QHF case.

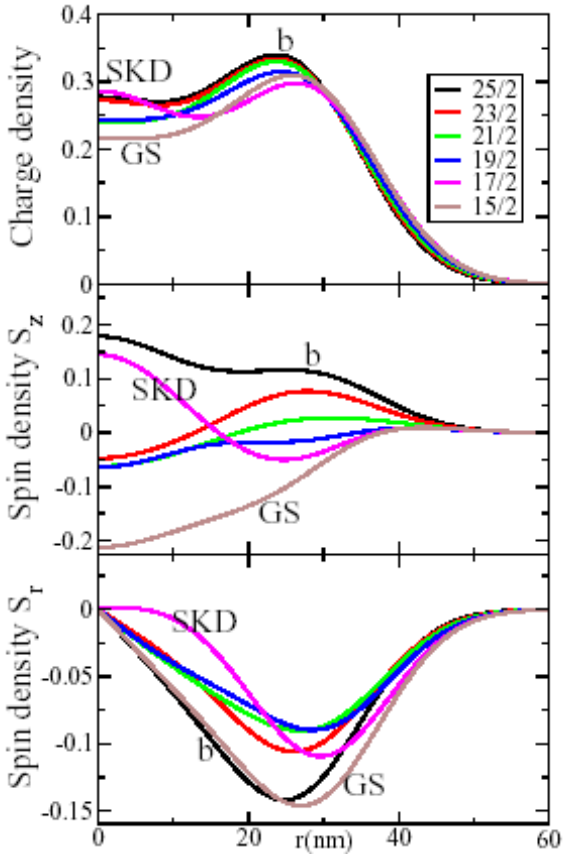

Figure 9: Charge density, azimutal spin density S_z, in plane spin density S_r in the radial direction at various J_z. Parameters are $N = 5$, $\alpha = 100$ meVÅ, $U = 13$ meV, and $\omega_d = 5$ meV.

An approach similar to that of Eq. (5) can be envisaged dealing with the SO as a perturbation. Coupled single particle levels have an energy difference $\delta = \epsilon_{0m+1} - \epsilon_{0m} = \omega_o - \omega_c/2$. The diagonalization implies a rotation in the 2-vector space $\{f_{0m}\chi_\uparrow, f_{0m+1}\chi_\downarrow\}$ by an angle γ such as $\tan 2\gamma = -2\alpha/\delta$. The mixing of the two states $(m, \uparrow)$ and $(m+1, \downarrow)$ is $j-$independent, within

our approximations, together with δ. This implies that the rotation angle γ keeps roughly constant in the radial direction (we arbitrarily relate radial distance from the center with the value j of a single particle orbital).

The spin excitation gives rise to an extra collective magnetization $\hat{z} \cdot \Delta\vec{\mathcal{M}}(r) \approx \langle 2\mu_B \Delta S_z(r) \rangle$, where $\mu_B = e\hbar/2m_e c$ and $\Delta S_z(r')$ is the difference in z-component of the local spin density between the FES and the GS. We have estimated the possible extra magnetic flux ϕ associated to the spin excitation, by integrating numerically the tangential component of the vector potential induced by the spin polarization of the dot, $a_\vartheta(r)$, along the circle γ of radius R at the dot boundary:

$$a_\vartheta(r) = \int_0^{2\pi} d\vartheta' \int_0^R \frac{dr'\, \vec{r}' \times \hat{z}}{|\vec{r} - \vec{r}'|} \frac{\partial \Delta\vec{\mathcal{M}}(r')}{\partial r'} \quad . \tag{13}$$

The flux $\phi = \int_\gamma R\, d\vartheta\, a_\vartheta(R)$ gives a result that is a small fraction of the flux quantum: $\sim 10^{-5}\phi_o$ (see Appendix). This order of magnitude can be understood by considering that the atomic unit of magnetic field strength is $h_a \sim \phi_o/a_B^2 = 2.35 \cdot 10^5$ Tesla which is threading here an area of roughly $(50\ \text{nm})^2$. This yelds a flux which is a factor of hundred larger than our result. However, a remarkable cancellation occurs here: according to Fig. 9, $3/2 \cdot h_a$ is squeezed in 1/4 of the area, while $-1/2 \cdot h_a$ is in the remaining 3/4 of the total area. Besides, inspection of the Table of Appendix shows that, at $B \approx B^*$, we get very close values of ϕ for $N = 2, 3, 4$. This is consistent with the fact that the FES has essentially one spin flipped at the origin and an increase of J_z by one, with little change in the orbital angular momentum.

By increasing the SO coupling α the spin density texture is squeezed closer and closer to the origin of the dot as shown in Fig. 10 and the energy cost of such a spin configuration increases. The energy cost is given by the gap between the FES and the GS appearing in Fig. 5 (inset).

Of course, there is no broken symmetry in the dot in contrast with what happens in the QHF, which is best described by the $O(3) - NL\sigma$ model. This spin exciton is not a topological excitation with a conserved charge, as the skyrmion is.

In the $O(3) - NL\sigma$ model the order parameter space is a sphere S_2 with antipodal points corresponding to parallel and antiparallel magnetization. On the other hand, the configuration space is a disk, but it can be compactified to a sphere S_2, provided that the point at infinity has the same magnetization. The homotopy group for the mapping of S_2 into S_2 for the finite energy solutions of the equation of motion for the magnetization is

$\pi_2(S_2) = \mathcal{Z}$, where $\mathcal{Z}$ is the group of integers, pointing out that the charge Q of Eq. (10) is conserved and discrete.

In the QD the SO coupling is needed to lower artificially the symmetry from separate conservation of M and S_z to conservation of $J_z = M + S_z$ only. The spin density of the GS is radially oriented at the dot boundary, what excludes that the coordinate space can be compactified to a sphere. Hence the topological classification of the lowest excited states is out of reach.

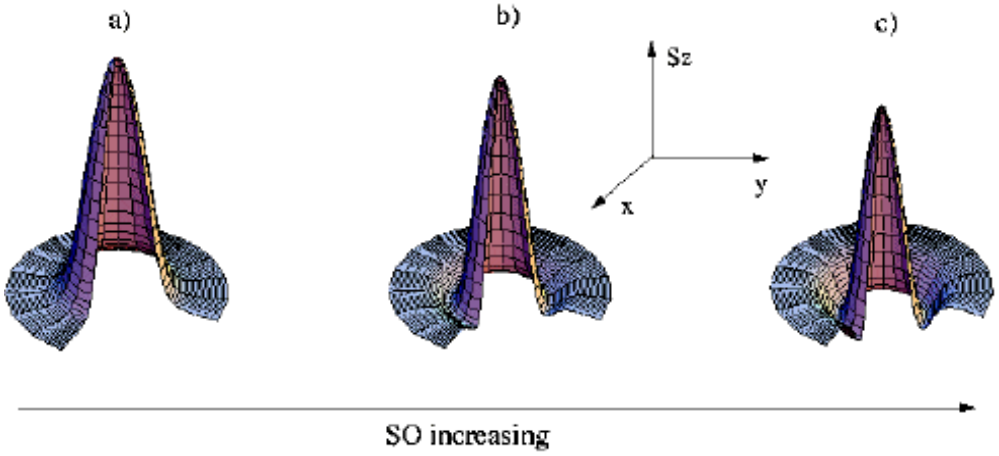

Figure 10: N=3 particles dot: FES spin density (arb.units) for a) α = 150 meVÅ, b) α = 250 meVÅ, c) α = 350 meVÅ. By increasing the SO there is a squeezing close to the center and some reduction of S_z.

6 FIR absorption and the crossover to the QHF state

We have argued that the FSP state of a disk shaped QD at $B = B^*$, in the vicinity of the Maximum Density Droplet condition, can be put into correspondence with the QHF. Increase in the electron number N and decrease in the absence of confinement potential ratio ω_d/ω_c apparently lead to the thermodynamic limit of the quantum Hall state.

We have shown by exact diagonalization of a few electron QD that the FSP state and the FES play the role of ferromagnetic GS of the QHF and the skyrmion excitation, respectively.

Equivalent interpretations of the skyrmion-like FES in FSP QD enforced by the presence of SO are as follows.

a) The SO moves opposite spin radially, thus expanding the effective dot surface and reducing the equivalent filling factor. This allows for the low lying FES with $\Delta J_z = 1$, in a way analogous to the QHF skyrmion state.

b) The SO acts as an effective magnetic field at right angle with the applied B field. This slightly reduces full spin polarization, what implies that some double occupancy of the single particle levels with an effective reduction of the equivalent filling factor as above.

Here we argue that the expected crossover to the QHF can be monitored by exciting the dot out of the GS into the FES with far infrared (FIR) radiation.

In fact, the GS and the FES are spaced by an energy of the order of meV, so that, by choosing an appropriate polarization of the radiation field, we can transfer the needed angular momentum and couple the two states. Increasing of the total angular momentum of $\Delta J_z = 1$ of the QD requires a right hand circularly polarized radiation.

The coupling hamiltonian in the dipole approximation can be written as:

$$H_{FIR} = \sqrt(2)\mathcal{A}_0(\omega)\hat{\epsilon}_R \cdot \vec{p}\, e^{i\omega t} + h.c. \tag{14}$$

where $\mathcal{A}_0(\omega) = A_0(\omega)/\sqrt{2}[exp(-i\omega t) + c.c.]$ (and $A_0(\omega)$ is the envelope function of the wavepacket in the ω-space, which we suppose to be very peaked around the ω frequency to simulate a monochromatic radiation) and $\epsilon_R = \hat{x} + i\hat{y}$ is the unit vector characterizing a right hand circularly polarized radiation. Typical wavelength of FIR are $1 \div 100$ μm while typical dot size are usually less then 100 nm: this assures that, in this case, dipole approximations holds to a high degree of accuracy.

Far infrared radiation is a common tool in large scale QD arrays (e.g. In QD's [35] or field-effect confined GaAs QD [36]). However, the usual outcome of FIR spectroscopy is rather poor, because Kohn 's theorem prevents the possibility of coupling radiation to degrees of freedom other than the center of mass coordinate.

Were this the case, we would have no chance of detecting the FES, which intrinsically has many-body nature.. However, the SO term in the Hamiltonian does not commute with the center of mass coordinate and disproves Kohn 's theorem.

We have calculated the dipole matrix element squared for the transition from GS to FES vs B. Our results are shown in Fig. 11(a) for $N = 2$ and Fig. 11(b) for $N = 4$, respectively. The dispersion of absorption peaks is artificial. Their detailed shape would yield direct access to the electron spin relaxation mechanisms that were mentioned in the Introduction. They require further

investigation. Here we concentrate on the height of the peaks: we find an increase of the expected intensity at the FSP point which marks the crossover to new states. As expected, the crossover sharpens with increasing N.

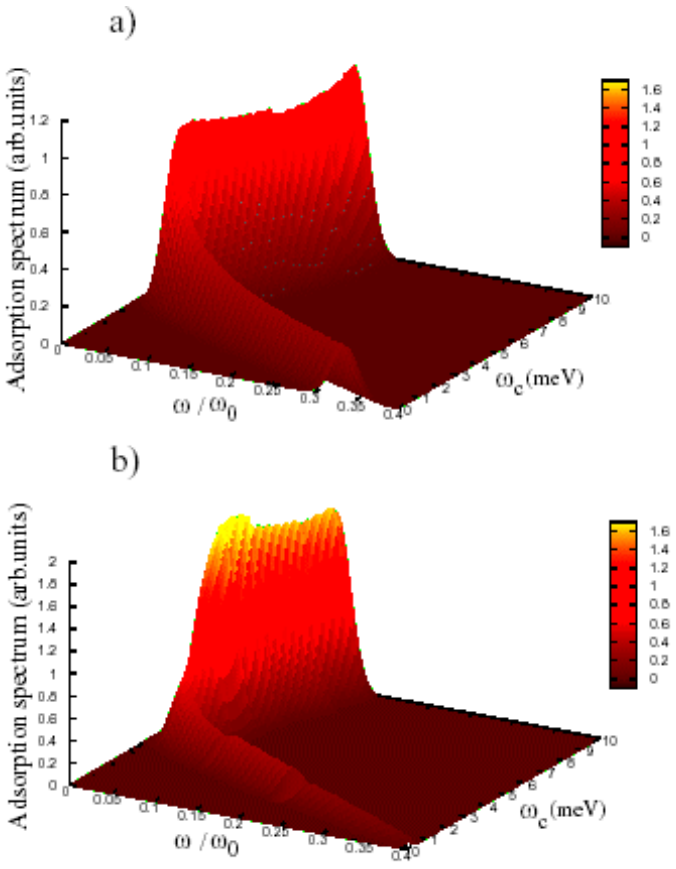

Figure 11: Absorption spectrum vs magnetic field for a) N=2 particles, b) N=4 particles.

7 Conclusions

In conclusion, it is possible to induce the transition between the FSP GS of a QD with SO and the FES by means of circularly polarized FIR radiation. The transition probability increases substantially, as soon as B drives the QD to the FSP GS. The FES has a spin flipped at the center of the dot.

Relaxation could take place due to hyperfine interaction with the underlying distribution of nuclear spins. On the other hand, the nuclear spins could be flipped when the spin exciton is excited. The possibility to exploit this technique to manipulate localized nuclear spins in coherent state devices is very appealing and should be explored.

Appendix. The reversed spin flux

The effective extra magnetic current density associated to the change in magnetization $\Delta\vec{\mathcal{M}}(r) \approx \langle 2\mu_B \Delta\vec{S}(r)\rangle$ due to the flipping of the spin between the GS and the FES is $c\vec{\nabla}\times\Delta\vec{\mathcal{M}}(r)$. Hence the tangential component of $\vec{a}(r)$, evaluated along a circle of radius $R \approx 80$ nm, is

$$a_\vartheta(R) = \int_0^{2\pi} d\vartheta' \int_0^R \frac{dr'\, \vec{r}' \times \hat{z}}{|\vec{R}-\vec{r}'|} \frac{\partial \Delta\mathcal{M}_z(r')}{\partial r'} \quad . \tag{15}$$

We use the representation of $1/|\vec{R}-\vec{r}'|$ in integer Bessel functions:

$$\int_0^{2\pi} d\vartheta' \frac{1}{|\vec{R}-\vec{r}'|} = 2\pi \int_0^\infty dk\, J_o(kR)\, J_o(kr') \quad , \tag{16}$$

and calculate numerically the integral. The result is a very tiny fraction of the flux quantum $\sim 10^{-5}\ hc/e$, but it is remarkable that, at $B \approx B^*$, we find very close values of ϕ for $N = 2, 3, 4$, according to the table:

N	2	3	4
GS	-1.575	-2.298	-2.743
FES	-0.117	-0.670	-1.168
FES - GS	1.458	1.628	1.575

In the table the fluxes ϕ are given for the GS and the FES, respectively, together with the difference between the two, for various N at $B \sim B^*$ in units of $10^{-5}\ hc/e$. The parameters here used are $\omega_d = 5$ meV, $U = 13$ meV, $\alpha = 250$ meVÅ.

References

[1] L.P. Kouwenhoven, D.G. Austing, S. Tarucha, Rep. Prog. Phys. **64**, 701 (2001); L.P. Kouwenhoven and C.M. Marcus, Phys. World **116**, 35 (1998); M.A. Kastner, Ann. Phys. (N.Y.) **9**, 885 (2000).

[2] *Semiconductor Spintronics and Quantum Computing*, Eds.: D.D. Awshalom, D. Loss and N. Samarth, (Springer Verlag, N.Y., 2002); *Quantum Phenomena in Mesoscopic Systems,* Proc. Int. Varenna School of Phys."E. Fermi", course CLI, Eds.: B.L. Altshuler, A. Tagliacozzo, V. Tognetti (IOS Press, Amsterdam, 2003).

[3] B. Jouault, G. Santoro, and A. Tagliacozzo, Phys. Rev. B **61**, 10242 (2000).

[4] H. Imamura, H. Aoki, and P.A. Maksym, Phys. Rev. B **57**, R4257 (1998).

[5] I.L. Aleiner, P.W. Brouwer, and L.I. Glazman, Phys. Rep. **358**, 309 (2002).

[6] D. Giuliano, B. Jouault, and A. Tagliacozzo, Europhys. Lett. **58**, 401 (2002).

[7] P. Stefanski, A. Tagliacozzo, and B. Bulka, Phys. Rev. Lett. **93,** 186805 (2004).

[8] D. Giuliano, P. Sodano, and A. Tagliacozzo, Phys. Rev. B **67**, 155317 (2003).

[9] A.V. Khaetskii and Y.V. Nazarov, Phys.Rev. B **61**, 12639 (2000); Phys. Rev. B **64**, 125316 (2001).

[10] B.I. Halperin, A. Stern, Y. Oreg, J.N.H.J. Cremers, J.A. Folk, and C.M. Marcus, Phys. Rev. Lett. **86**, 2106 (2001).

[11] A. Imamoglu, E. Knill, L. Tian, and P. Zoller, Phys. Rev. Lett. **91**, 017402 (2003).

[12] R. Tycko, S.E. Barrett, G. Dabbagh, L.N. Pfeiffer, and K.W. West, Science **268**, 1460 (1995).

[13] Y. Ishikawa and H. Fukuyama, J. Phys. Soc. Jpn. **68**, 2405 (1999).

[14] E.H. Aifer, B.B. Goldberg, and D.A. Broido, Phys. Rev. Lett. **76**, 680 (1996).

[15] P. Lucignano, B. Jouault, A. Tagliacozzo, and B.L. Altshuler, Phys.Rev. B **71**, 121310(R) (2005).

[16] Y.B. Lyanda-Geller, I.L. Aleiner, and B.L. Altshuler, Phys. Rev. Lett. **89**, 107602 (2002).

[17] J.M. Taylor, C.M. Marcus and M.D. Lukin, Phys. Rev. Lett. **90**, 206803 (2003).

[18] A.S. Bracker, E.A. Stinaff, D. Gammon, M.E. Ware, J.G. Tischler, A. Shabaev, Al.L. Efros, D. Park, D. Gershoni, V.L. Korenev, and I.A. Merkulov, cond-mat/0408466.

[19] V. Privman, I.D. Vagner, and G. Kventsel, Phys. Lett. A **236**, 141 (1998).

[20] T. Maniv and Y.A. Bychkov, HAIT J. Sci. Eng. **1**, 220 (2004).

[21] D. Giuliano, B. Jouault, and A.Tagliacozzo, In: *Proceedings of Macroscopic Quantum Coherence and Computing*, Eds.: P. Silvestrini and D. Averin (Kluwer Academic, N.Y., 2001).

[22] S. Tarucha, D.G. Austing, T. Honda, R.J. van der Hage, and L.P. Kouwenhoven, Phys. Rev. Lett. **77**, 3613 (1996).

[23] S.A. Mikhailov and N.A. Savostianova, Phys. Rev. B **66**, 033307 (2002); M.B. Tavernier, E. Anisimovas, F.M. Peeters, B. Szafran, J. Adamowski, and S. Bednarek, Phys. Rev. B **68**, 205305 (2003).

[24] P. Lucignano, B. Jouault, and A. Tagliacozzo, Phys. Rev. B **69**, 045314 (2004).

[25] O. Klein, C. de C. Chamon, D. Tang, D.M. Abusch-Magder, U. Meirav, X-G. Wen, M.A. Kastner, and S.J. Wind, Phys. Rev. Lett. **74**, 785 (1995); O. Klein, D. Goldhaber-Gordon, C. de C. Chamon, and M.A. Kastner, Phys. Rev. B **53**, 4221 (1996).

[26] T.H. Oosterkamp, J.W. Janssen, L.P. Kouwenhoven, D.G. Austing, T. Honda, and S. Tarucha, Phys. Rev. Lett. **82**, 2931 (1999).

[27] L.P. Rokhinson, L.J. Guo, S.Y. Chou, and D.C. Tsui, Phys. Rev. Lett. **87**, 166802 (2001).

[28] C. de Chamon and X.G. Wen, Phys. Rev. B **49**, 8227 (1994); S.M. Reimann, M. Koskinen, M. Manninen, and B.R. Mottelson, Phys. Rev. Lett. **83**, 3270 (1999).

[29] S.L. Sondhi, A. Karlhede, S.A. Kivelson, and E.H. Rezayi, Phys. Rev. B **47**, 16419 (1993)

[30] A.H. MacDonald, In: NATO ASI *Quantum Transport in Semiconductor Submicron Structures*, Ed.: B. Kramer (Kluwer, Berlin, 1996).

[31] B.I. Halperin, Helv. Phys. Acta **56**, 75 (1983).

[32] H.A. Fertig, L. Brey, R. Côté, A.H. MacDonald, A. Karlhede, and S.L. Sondhi, Phys. Rev. B **55**, 10671 (1997); M. Abolfath, J.J. Palacios, H.A. Fertig, S.M. Girvin, and A.H. MacDonald, Phys. Rev. B **56**, 6795 (1997).

[33] A.A. Balavin and A.M. Polyakov, JETP Lett. **22**, 245 (1975); A.M. Polyakov, Phys. Lett. B **59**, 79 (1975).

[34] E.I. Rashba, Fiz. Tverd. Tela **2**, 1224 (1960) [Sov.Phys. - Solid State **2**, 1109 (1960)]; Y.A. Bychkov, E.I. Rashba, J. Phys. C **17**, 6039 (1984).

[35] M. Fricke, A. Lorke, J.P. Kotthaus, G. Medeiros-Ribeiro, and P.M. Petroff, Europhys. Lett. **36**, 197 (1996); P. Junker, U. Kops, U. Merkt, T. Darnhofer, and U. Rossler, Phys. Rev. B **49**, 4794 (1994).

[36] R. Krahne, V. Gudmundsson, G. Heyn, and D. Heitmann, Phys. Rev. B **63**, 195303 (2001).